J Mater Sci: Mater Electron (2017) 28:13426–13435
DOI 10.1007/s10854-017-7181-2

Enhancement of silicon nanowire opto-electric properties by combining acid vapor etching and lithium pore-filling

Chohdi Amri[1,2,3] · Rachid Ouertani[2] · Abderrahamn Hamdi[1,2,3] · Hatem Ezzaouia[1]

Received: 6 January 2017 / Accepted: 19 May 2017 / Published online: 23 May 2017
© Springer Science+Business Media New York 2017

Abstract In this paper, we report a novel method combining acid vapor etching (AVE) and Lithium (Li) pore-filling aiming to enhance the opto-electrical properties of silicon nanowires (SiNWs). Images provided by both scanning and transmission electron microscopies (SEM and TEM) show that, the silver-Assisted Chemical Etching (Ag-ACE) method provides uniform and vertically aligned SiNWs with smooth sidewalls. AVE treatment leads to the formation of thin porous silicon (pSi) layer covering the initially solid SiNW sidewalls without affecting their initial length. The as-prepared porous SiNWs (pSiNWs) exhibit a quite strong photoluminescence (PL) band centered on 2 eV. An additional immersion of pSiNWs in LiBr aqueous solution leads to a significant change in the surface chemistry and a stable PL emission with fourfold increase in the intensity. The total reflectivity decreases with Li concentration and reaches 1% in the visible range. Simultaneously, the minority carrier lifetime (τ_{eff}) of pSiNWs is enhanced from 1.48 to 7.1 µs due to the formation of a stable passivation layer and the saturation of dangling bands. The dark I–V measurement shows a significant decrease of the series resistance from 340 to 85 Ω.

✉ Chohdi Amri
Chohdiamri@gmail.com

[1] Laboratory of Semi-conductors, Nano-structures and Advanced Technologies, Research and Technology Centre of Energy, Borj-Cedria Science and Technology Park, BP 95, 2050 Hammam-Lif, Tunisia

[2] Photovoltaic Laboratory, Research and Technology Centre of Energy, Borj-Cedria Science and Technology Park, BP 95, 2050 Hammam-Lif, Tunisia

[3] Faculty of Science of Bizerte, University of Carthage, 7021 Zarzouna, Tunisia

1 Introduction

Recently, pSiNWs produced by Ag-ACE have been extensively studied due to its high potential for a variety of applications for instance opto-electronic devices [1], sensors [2] and solar cells [3]. The appearance of porous structure along the SiNW sidewalls is strongly related to etching parameters such as etching duration [4], H_2O_2 concentration [5] and doping level of the starting silicon (Si) wafer [6]. Since the discovery of the visible PL originating from pSi layer by Canham [7], several experimental, theoretical works and many possible mechanisms have been reported to highlight the origin of these intriguing radiations [8–11]. The foremost adopted models are the quantum confinement and the interfacial oxide-related defect models [12]. On the other hand, a high PL emission intensity is detected from pSiNWs only when they are grooved in a substrate having a resistivity lower than 0.005 Ω cm [13]. However, low resistivity starting Si wafers have a high impurity doping levels which limit seriously the electrical characteristics of the elaborated pSiNWs. To thwart this impediment, lightly doped Si wafer was selected as a starting material. In this case, porous structure along the SiNWs cannot be conventionally engineered [14]. In this topic, some works have generated a porous layer on SiNW sidewalls by submitting them to post-treatments such as electrochemical anodization [15] or stain etching [16]. In a previous work [17], we successfully elaborated a thin porous layer along SiNW sidewalls by exposing them to a hot acid vapor. The as-prepared pSiNWs exhibit interesting optical proprieties but limited electric performance.

It has been previously reported that surface passivation enhances significantly the opto-electric proprieties of the Si nanostructures. Lin et al. [18] and later Leontis et al. [19] have established that the post-chemical treatment of

pSiNWs using selenium and HF, respectively, leads to an important increase of the PL signal. However, these investigations have used highly doped Si wafers as a starting material. On the other hand, Li et al. [20] and Kato et al. [21] have enhanced the minority carrier life time of the SiNWs by the deposition of a thin Si–H amorphous layer and alumina (Al_2O_3) films, respectively. However, these passivating layers are deposited by sophisticated equipments (PECVD and ALD) related on expensive precursor.

In this work, starting form lightly doped Si substrates, we elaborate solid SiNW arrays. Aiming to improve their opto-electric proprieties, SiNW arrays have been exposed, in the first step, to hot acid vapor to generate a thin porous layer. Secondly, the as-prepared pSiNWs are passivated by a short dipping in aqueous LiBr solution followed by a rapid thermal processing (RTP).

2 Experimental

2.1 Synthesis of solid SiNWs arrays

In this work, p-type Si (100) wafers with resistivity of 14–25 Ω cm and 450 µm thickness are employed to fabricate SiNWs. First, Si wafers are cleaned by dipping in acid solution mixture of HNO_3: 64%, HF: 16%, CH_3COOH: 20% for 30 s then copiously rinsed in deionized water and dried. The cleaned substrates are immersed in an aqueous solution of 4.8 M HF and 0.02 M $AgNO_3$ for 1 min to induce the formation of silver nanoparticles (AgNPs) netlike films. We note that the rear sides of cleaned substrates are protected by sticking them to an acid resistant adhesive shred to avoid the deposition of AgNPs and as a consequence the formation of SiNWs. In the second step, the substrates are immersed in aqueous solution mixture of 4.8 M of HF and 0.2 M of H_2O_2 during 5 min. The as-prepared brown samples were subsequently immersed copiously in concentrated nitric acid to remove silver particles. After a final rinsing and drying operations, the substrates are covered with a black layer of SiNWs.

2.2 Synthesis and passivation of pSiNW arrays

Solid SiNW arrays were made porous by using the AVE technique. The AVE is a simple method originated for the first time by Saadoun et al. [22] and re-examined in our recent work [17]. According to this technique, the as-prepared SiNW samples are exposed to acid vapors, issued from a hot solution mixture of HNO_3/HF:1/3 for a fixed duration 45 s. To control the exposure duration, the samples are immediately dipped in deionized water after 45 s of vapor exposure. So that etching reaction is stopped. Furthermore, in order to study the passivation effect of Li pore-filling, the freshly prepared pSiNWs are immersed in an aqueous solutions of lithium bromide (LiBr) with different concentrations C_i ($i = 1–3$): 0.05; 0.1 and 0.2 M, for 10 min at atmospheric conditions, respectively. As a final step, samples have been submitted to a thermal annealing treatment in an infrared furnace under nitrogen atmosphere. The annealing duration and temperature are fixed to 15 min and 200 °C, respectively.

3 Characterization

Scanning Electron Microscope (SEM, HITACHI 4800) and Transmission Electron Microscope (TEM, TECNAI G2F20) were employed for the morphology study. The reflectivity of samples after each processing step was measured by LAMBDA 950 de Perkin Elmer UV/Vis/NIR Spectrophotometer equipped with an integrating sphere in the 250–1100 nm wavelength range. PL spectroscopic analyses of pSiNWs and the LiBr-deposited pSiNWs samples were performed at ambient temperature with 4765 Å laser. The FTIR spectra were recorded using Nicolet MAGNA-IR 560 Spectrometer with a resolution of 2 cm^{-1}. The variation of the effective minority carrier lifetime, before and after LiBr deposition, was evaluated using the Sinton WCT-120 lifetime tester.

4 Results and discussion

4.1 Structure and morphology

Figure 1 exhibits SEM images of SiNWs before and after AVE treatment. SiNWs prepared via two-step Ag-ACE are distributed uniformly and vertically to the surface with a length of about 3 µm. The formation of the vertical SiNWs is governed by the Si substrate orientation [23]. After magnification (Fig. 1b), SiNW surface is relatively smooth. This is mainly due to short etching duration (10 min), the low doping density (~10^{14} cm^{-3}) and the low H_2O_2 concentration (0.2 M). In fact, dopant atoms incorporated in Si wafer are point defects which are considered as nucleation sites in the AgNPs re-deposition process. As the etching duration increases, AgNPs are expected to nucleate and re-deposit on the SiNW surface leading to new lateral etching pathways and prevent the formation of porous structure [24]. However, in lightly doped Si substrate, the re-deposition of Ag^+ ions during etching is limited by the low doping level and low surface defects such as steps and kink sites. After AVE treatment (Fig. 1c, d), a thin porous structure appears along the SiNW sidewalls without affecting the SiNWs diameter.

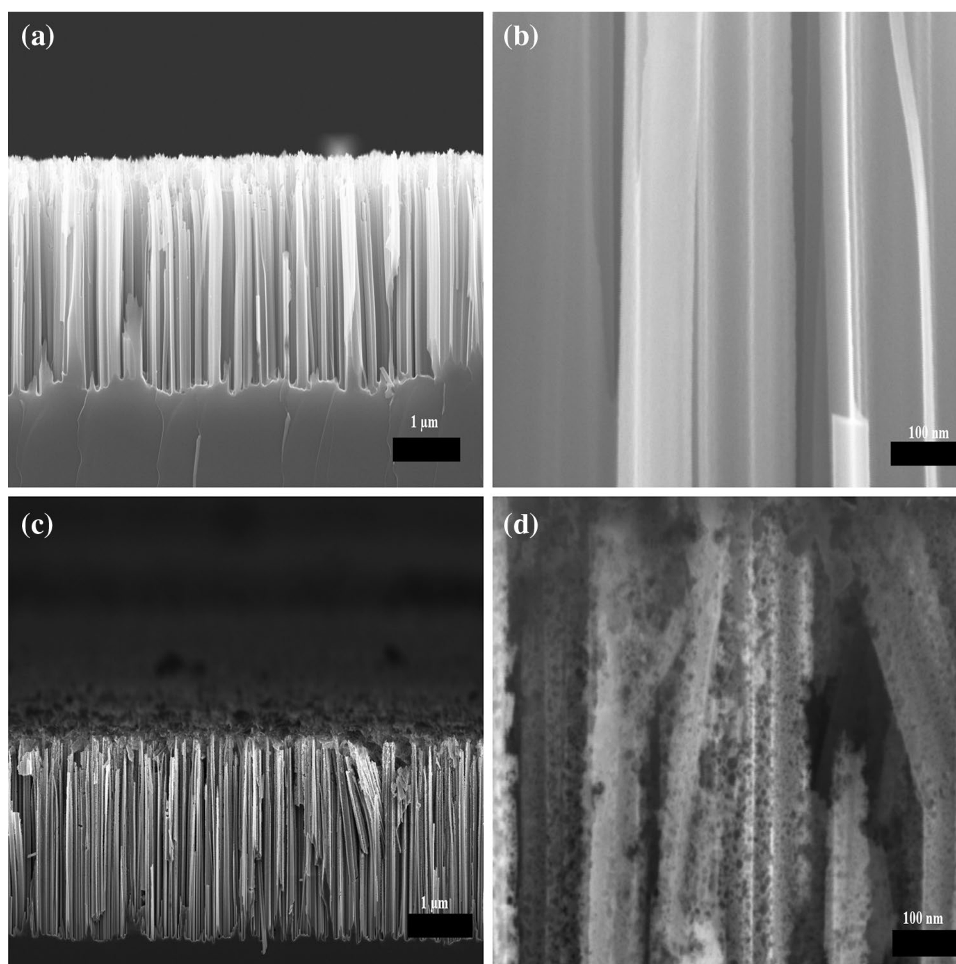

Fig. 1 SEM images of SiNWs before (**a, b**) and after (**c, d**) AVE treatment

Figure 2 displays TEM images of individual SiNW before the AVE treatment. SiNW elaborated via Ag-ACE has a constant diameter almost 100 nm and smooth sidewalls. Conversely, after exposing to HF/HNO_3 hot vapors (Fig. 2b), the SiNW sidewalls are covered with a thin porous layer where its diameter has not been affected by etching and still around 100 nm. The image magnification on both SiNW sidewall (Fig. 2c) and core (Fig. 2d), we observe SiNCs having a wire shape rippled in section and interconnected or free Si quantum dots with a diameter raging between 3 and 5 nm.

4.2 FTIR spectroscopic analysis

FTIR measurement shown in Fig. 3 has been conducted to identify the chemical species on SiNW arrays before and after subsequent AVE and Li pore-filling. In Fig. 3I, SiNWs without any additional treatment reveal a low density of Si–O–Si species situated at 1060, 1106 and 1120 cm^{-1}. The appearance of these bands could be attributed to the incorporation of oxygen atoms during the HNO_3 treatment intended to remove residual AgNPs. After AVE treatment, SiNW arrays become porous as observed by TEM images. The corresponding FTIR spectrum shows the persistence of oxygen bands exhibiting nearly the same order of magnitude. The hydrides Si–H_x in the stretching modes ($x = 1$, 2 and 3) are situated at 2085, 2112, and 2143 cm^{-1}, respectively and attributed to the formation of pSi layer on the SiNW sidewalls [25]. At the high energy vibration modes (Fig. 3II), we record the O_2Si–H and O_3Si–H_2 bands situated at 2251 and 2198 cm^{-1}, respectively. FTIR spectra of pSiNW samples immersed in Li aqueous solution show a significant steady enhancing of the peak intensities (Si–O–Si and O_xSi–H_y) related to oxygen incorporation. Simultaneously a net dwindling of Si–H_x band is observed as the result of the facile incorporation of oxygen in the Si–Si–H groups. This assumption is confirmed by the formation of Si–O–Si–H and its evolution to O_xSi–H_y bands localized at 939 and 947 cm^{-1}, respectively. So, the Li treatment accelerates the oxidation process through the replacement of the hydrogen atoms by the oxygen atoms according to the following reactions:

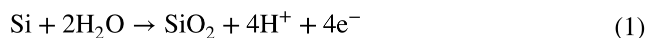

$$Si + 2H_2O \rightarrow SiO_2 + 4H^+ + 4e^- \quad (1)$$

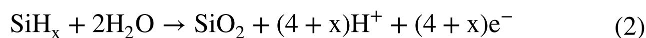

$$SiH_x + 2H_2O \rightarrow SiO_2 + (4 + x)H^+ + (4 + x)e^- \quad (2)$$

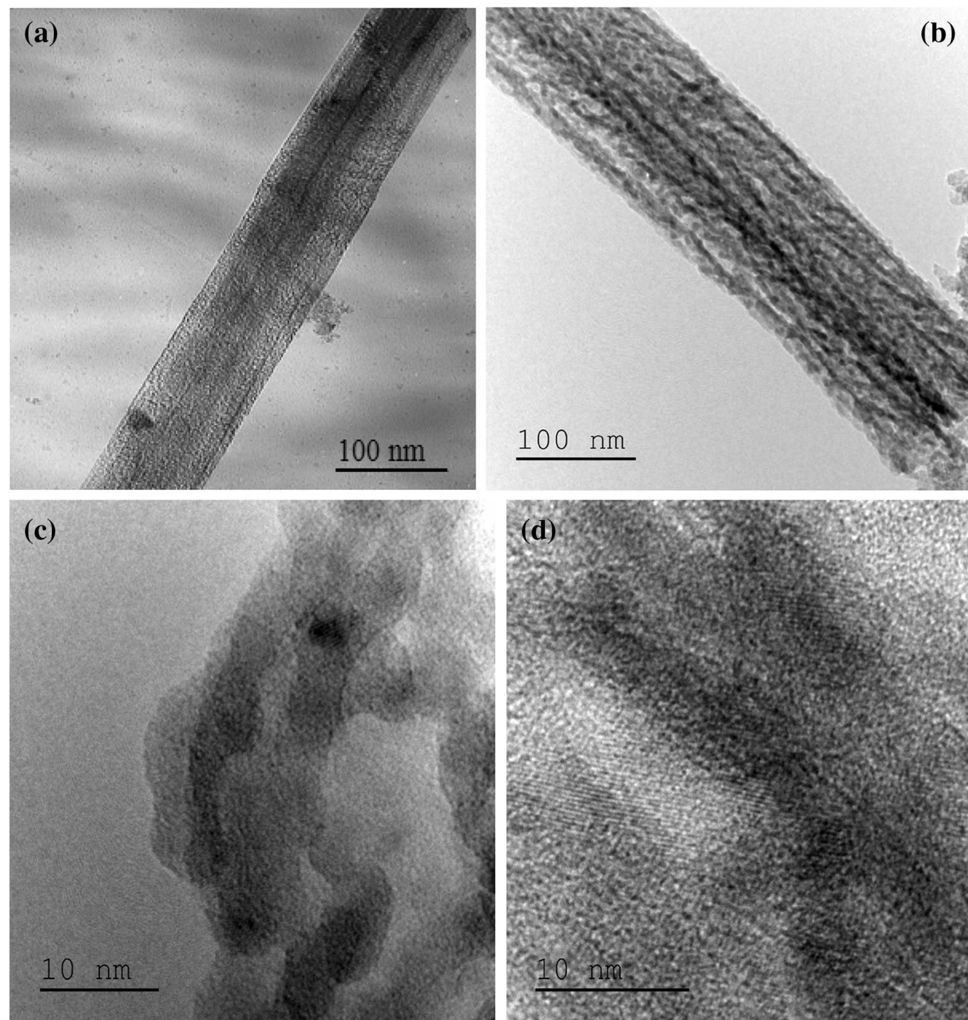

Fig. 2 TEM images of individual: **a** smooth and **b** porous SiNW. HRTEM of the porous SiNW morphology: both **c** surface and **d** core patterns show interconnected Si quantum dots and Si quantum wires with rippled sections

On the other hand, the appearance of new peaks situated at 468, 660, 830, 850, and 880 cm^{-1} subsequently to the Li pore-filling has been reported in previous works conducted by Zarroug et al. [26] and later by Haddadi et al. [27]. These peaks are attributed to Li–O–Si bands. The deposition mechanism of pore-filling with Li atoms depends essentially on the Li solution concentration and the pSiNW surface properties. A nucleation step is initiated from a finite number of nuclei site sites generated at the early stage of immersion even in lightly concentration solution. At a certain nuclei site, a locally oxidation of Si atoms occurs when an electron is extracted from Si to reduce the Li^+ ions according to the following reaction:

$$Li^+ + e^- \rightarrow Li \quad (3)$$

The electrons released by the anodic oxidation are supplied to the metal ions through the deposited metal resulting in the growth of the crystals. The formation of a thick Li film requires a long-lasting immersion in the plating solution allowing the growth mechanism to take over the nucleation phase. The growth rate is slows down considerably as the pSi layer is completely covered with a Si oxide shell. At this stage, the plating solution is no longer in contact with the Si surface so that the displacement reaction between the alkali Li and the Si atoms is stopped.

4.3 PL spectroscopic analysis

4.3.1 Effect of Li concentration

Figure 4 shows the PL spectra of SiNWs, pSiNWs and pSiNWs immersed in Li aqueous solution with different concentrations (C_1, C_2, and C_3). In our experimental conditions, SiNWs with a diameter around 100 nm and a smooth sidewalls do not show any PL emission, it behave like bulk Si that has an indirect band gap. After AVE treatment, pSiNWs exhibit a PL peak at room temperature localized around 2 eV. We suggest that PL emission originates from the porous structure observed by TEM in Fig. 2. According to the quantum confinement model, silicon nanocrystallites

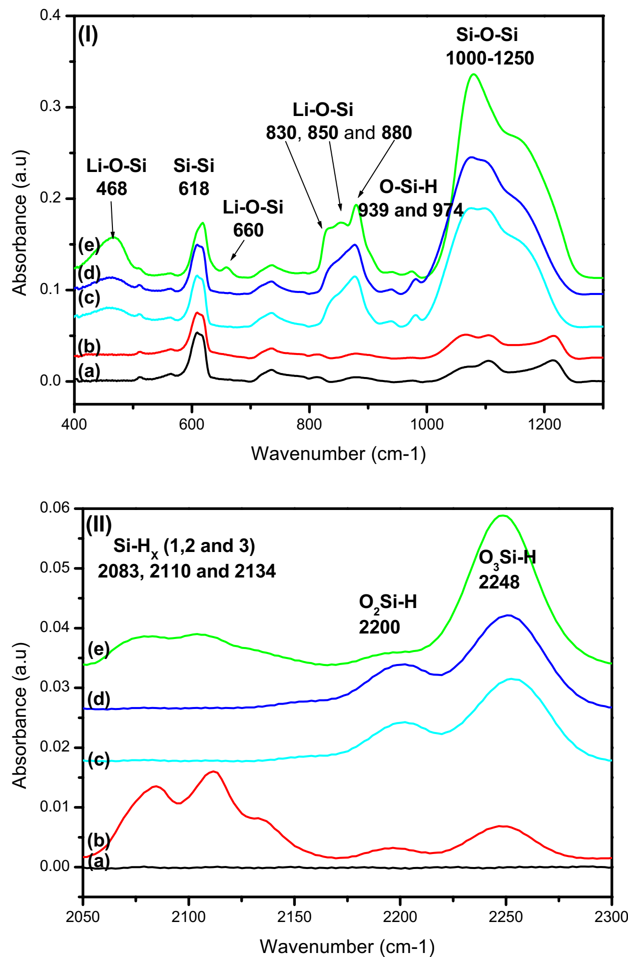

Fig. 3 FTIR absorption spectra in the range of **I** 400–1200 and **II** 2050–2400 cm^{-1} of (*a*) SiNWs (*b*) pSiNWs and pSiNWs immersed in LiBr aqueous solution with different concentrations: (*c*) C_3, (*d*) C_2 and (*e*) C_1

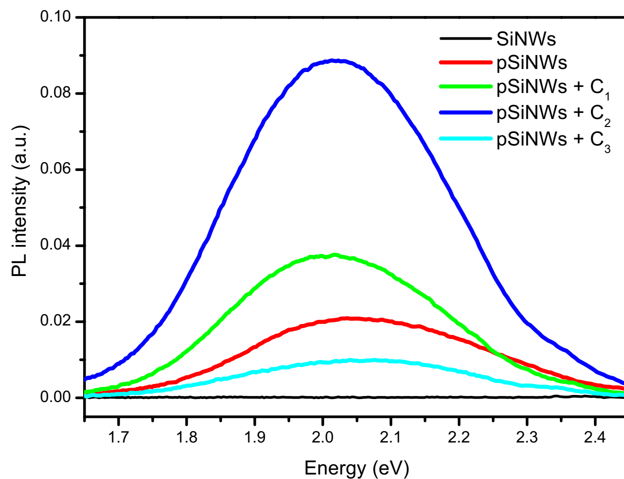

Fig. 4 PL spectra of (*a*) SiNWs, (*b*) pSiNWs and pSiNWs immersed in LiBr aqueous solution with different concentrations: (*c*) C_3, (*d*) C_2 and (*e*) C_1

(SiNCs) smaller than the dimension of free exciton box (5 nm) are named quantum dots (QDs) act as quantum wells. Within these SiNCs a strong quantum confinement starts to occur leading to an increase of the overlap between electron and hole wave functions in k-space, which leads to an increase of the radiative recombination probability and the appearance of PL emission. The broad emission may be attributed to broad size distribution of the SiNCs along pSiNWs. After immersing in LiBr aqueous solution, the PL intensity increases. For a relatively low concentration (C_1), the Li-free SiNCs and the oxide species would exist in either islands or isolated clusters leaving enough dangling bands and inducing a low oxide quality. Despite that we observe a remarkable PL enhancement, nearly twofold more intense than that of Li-free pSiNW arrays. The highest PL peak intensity is recorded for moderated concentration (C_2) and shows fourfold enhancement.

The PL behavior is thoughtful to the effective surface recombination velocity and the band bending at the surface [28]. Dangling bands generated during the AVE at the surface of SiNCs and interface Si/SiO_2 give rise to electronic states within the band gap. Electrons originated from the Si bulk fill up these states to Fermi level. On the other hand, the accumulation of charges at the surface creates an electric field leading to the formation of depletion region and to the bending of the valence and conduction edge bands. Electron–hole pairs generated in this region are kicked away by the electric field, giving preference to the non-radiative recombinations and prohibiting radiative ones. As a result dangling bands are responsible of the PL quenching [29]. The Li pore-filling treatment of pSiNWs passivates a high dangling band density and quenches as a result a big part of the non-radiative recombination centers through the substitution of the non stable hydride bands (Si–H_x) by more stable Si–O–Si and Li–O–Si bands. In addition, the porous structure along the SiNW sidewalls could be considered as a network of Si–SiO_x core–shell. The SiO_x density increases with the Li concentration and leads to the amplification of under-coordinated O atom bonded to a single Si atom displaying a hole in its non-bonding 2p orbital (–Si–O^-) so-called as Non Bridged Oxygen Hole Centers (NBOHCs) [30]. The enhancement in the PL intensity is attributed to increase of the NBOHCs. This important enhancement in the PL intensity is accompanied by a low red shift of about 0.02 eV. The oxidation of SiNCs leads to the shrinking of the Si size. Subsequently and according to the quantum confinement model, a blue-shift of the PL peak should take place [7]. Surprisingly, this view point appears contradictory to our results. To understand this discrepancy, we have to consider two different PL origins: the quantum confinement and the interfacial NBOHCs. According to Koch [31], carriers are created with the quantum confined SiNCs and the recombination occurs at the

surface originating from Si band tail states created at the surface by strain and disorder. Since the presence of hydrogen affect the position of band tail states, the observed red-shift should be associated with the loss of hydrogen within the NBOHCs after the dipping [32].

However, when the Li concentration exceeds C_2, an opposite trend is observed. The PL intensity steadily decreases by three orders of magnitude accompanied by a slight blue-shift. This PL behaviour could be explained as follow. At high Li concentration, the Si is no longer in contact with the solution. The electrons keep moving from Si to Li^+ ions through Li nanoparticles. As this local displacement proceeds, the Li nanoparticles grow up to large nano-clusters that ultimately aggregate towards forming a relatively thick Li layer. In that case, the incident exciting light is largely reflected before reaching the active pSi layer. Additionally, the high Li concentration enhances the oxidation rate and induces the decrease of the overall SiNC density by the total oxidation of small SiNCs.

On the other hand, the observed PL blue-shift is attributed to the reduction of the SiNC sizes induced by the deep oxidation of their core. In brief, Li treated pSiNWs luminesce through the competition of two PL mechanisms: quantum confinement and surface state effects. Wolkin et al. [12] reported the same conclusion after staying the PL origin related to pSi.

4.4 Effect of natural aging days

It has been generally reported in the literature that PL emission from pSi is not stable in ambient air during several months [33, 34]. For that, the effect of natural aging days (120 days) has been carried out to reveal the impact of Li post-treatment on the stability of pSiNW PL emission. Figure 5 exhibits the evolution of the PL intensity of pSiNWs and pSiNWs treated with Li during 120 days. As depicted in Fig. 5 a, the PL intensity of pSiNWs decreases as function of aging days accompanied with a slight blue shift. These two observations are explained by the chemical instability of the pSiNWs surface and the decrease in SiNCs size during the air exposure by the impact of the natural oxidation. In this case, the natural oxidation helps the replacing of H-terminated surface with O-terminated surface. This indicates that O-termination plays a key role in the degradation and the instability of the PL intensity by the generation of non-radiative recombination centers that lead to a significant PL quenching. On the other hand, pSiNWs treated with Li exhibit a stable PL emission during the 4 months due to the replacement of instable hydride bands by a more stable Si–O–Si and Si–O–Li bands as discussed in Sect. 4.2. The PL peak position remains fixed around 2 eV. So, the Li passivation acts as a protecting layer that prevents the decrease in the SiNC size.

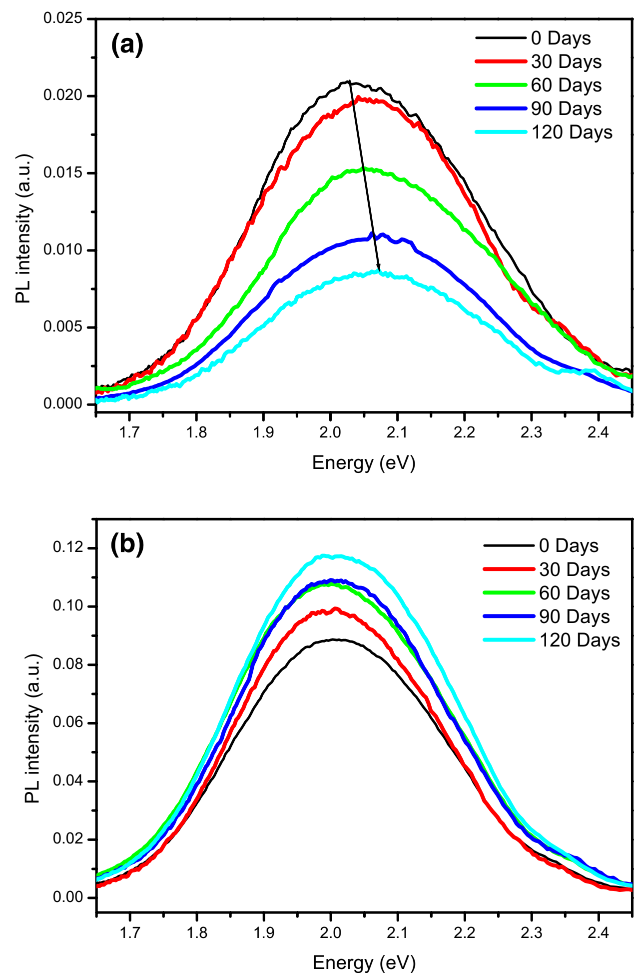

Fig. 5 Evolution of the PL intensity of **a** pSiNWs and **b** pSiNWs treated with LiBr during natural aging days

4.5 Total reflectivity analysis

Figure 6 shows the total reflectivity spectra of Si substrate before and after successive chemical treatments with AVE and Li pore-filling at different concentrations are recorded in the wavelength range 300–1100 nm. The reflectivity of non-treated Si substrate is about 34%. This relatively high value is due to the smooth surface and the absence of incident light trapping structure. After the elaboration of vertical SiNWs, a significant decrease in the reflectivity is obtained from 34 to 6% due to the high surface to volume ratio of the SiNWs enabling light trapping through the multiple scattering of sunlight between the wires [35]. The AVE of the vertical SiNWs decreases the reflectivity form 6 to 4%. This result is explained by the change of the SiNWs morphology and to the gradual increase in the refractive index due to the generation of a thin porous layer. Figure 6b shows a gradual decrease of

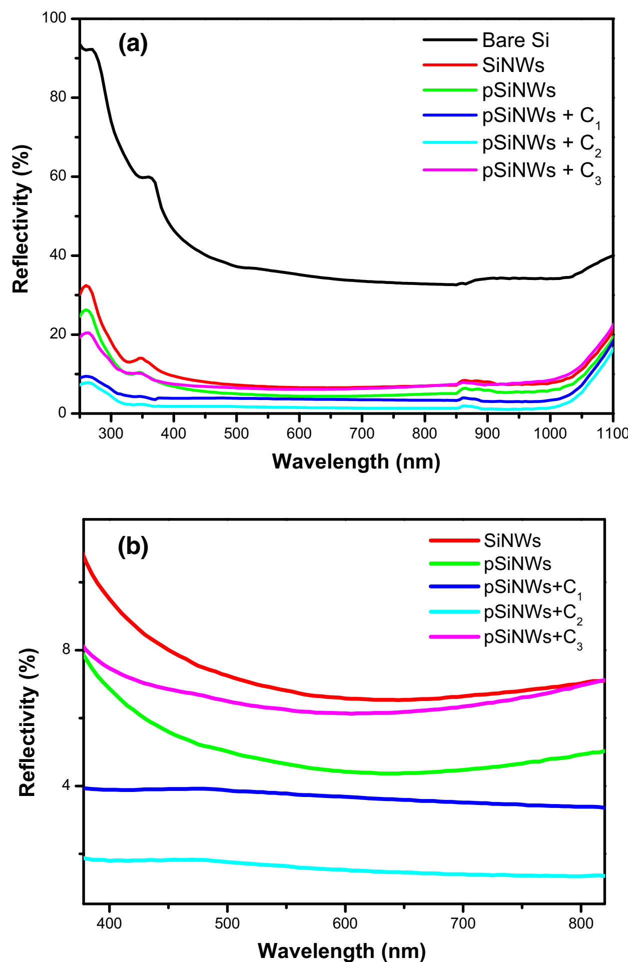

Fig. 6 Reflectivity spectra of SiNWs before and after AVE treatment and Li treatment with different concentration exhibited in the range: **a** 250–1100 and **b** 400–800 nm

the reflectivity as a function of the increase in Li concentration that reaches its minimum at a concentration equal to C_2. This result is attributed to the enhancement of the surface roughness by the formation of lithium thin layer [36]. In addition, the Li layer has a low refractive index (n_{Li} ~ 1.784) comparing to Si (n_{Si} ~ 3.6 at 600 nm) which allows as considering Li as an appropriate material for the anti-reflection layer of incident light. We note that n_{Li} is near the refractive indexes of the frequently used materials such as Al_2O_3 (n = 1.8–1.9) [37], SiO_2 (n = 1.4–1.5) [38], Si_3N_4 (n = 1.9) [39] and SiO_2–TiO_2 (n = 1.8–1.96) [40]. Thereby, both the nano-structured surface and the deposited Li layer reduce drastically the optical losses caused by reflections. However when exceeding this concentration the reflectivity starts to increase. We attribute this observation to the formation of thick Li layer that reflects the incident light before reaching the active porous silicon.

4.6 Minority carrier lifetime variation

The lifetime of the minority carriers is the average time between creation and further recombination of an electron–hole pair. In p-type Si, minority carriers are electrons. It is unanimously recognized that recombination happen through deep traps lying within the energy band gap. Either defects in the bulk close to the surface or unsatisfied bands on the surface create these traps. It has also been widely suggested that such traps can pin the Fermi level at the free semiconductor surface. We use the Sinton WCT-120 set up to perform contactless measurements of minority carrier lifetime in treated Si substrates. A flash lamp injects electron–hole pairs into the substrate. Then, an inductively coupled radio-frequency bridge monitors the carrier density decay. Effective surface recombination velocity S_{eff} is associated to effective carrier lifetime τ_{eff} which is given by the following Eq. (4) [41]:

$$\frac{1}{\tau_{eff}} = \frac{1}{\tau_b} + \frac{2S_{eff}}{W} \tag{4}$$

This Eq. (4) has been established assuming a high value of the bulk lifetime (τ_b) so that the entire recombination activities is considered to occur on the SiNWs surface. W is wafer thickness. The upper limit of S_{eff} is deduced using the following equation:

$$S_{eff} \leq \frac{W}{2\tau_{eff}} \tag{5}$$

As seen in Table 1, Ag-ACE technique produces solid SiNWs having τ_{eff} as low as 1.3 µs and S_{eff} as high as 17,308 cm s^{-1} comparing to the reference sample (τ_{eff} = 2.2 and S_{eff}= 10,227 cm s^{-1}). This behavior may be explained by a high-generated density of dangling bands resulting from unpaired valence electrons. This high dangling band density increases deep-level traps causing serious surface recombination [42]. In addition, it has been states that even a post cleaning of the wires with nitric acid does not remove totally residual silver nanoparticles which contribute to increase the recombination centers in the forbidden band. After AVE, pSiNWs show a slight increase in τ_{eff} (from 1.3 to 1.5 µs) due to the hydrogen passivation. After immersing in LiBr aqueous solution, τ_{eff} of pSiNWs has been significantly enhanced to reach 7.1 µs at the moderated concentration (C_2). As a result S_{eff} has been considerably reduced to 3169 cm s^{-1} leading to a high surface quality improvement. This is due to the plugging of dangling bands with the coordination of Li atoms to the Si atoms through the oxygen (Li–O–Si and Li–O–Li bands), as described in FTIR measurements (Fig. 3) and by producing a high quality oxide film with a low surface state density. As a conclusion, Li treatment provides a passivation

Table 1 Effect of Li pore-filling on τ_{eff} and S_{eff} of pSiNWs

Samples	Effective minority carrier lifetime τ_{eff} (µs)	Effective surface recombination velocity S_{eff} ($cm\ s^{-1}$)
Reference	2.2	10,227
SiNWs	1.3	17,308
pSiNWs	1.5	15,000
pSiNWs + C_1LiBr concentration	4.8	4688
pSiNWs + C_2 LiBr concentration	7.1	3169
pSiNWs + C_3 LiBr concentration	6.8	3309

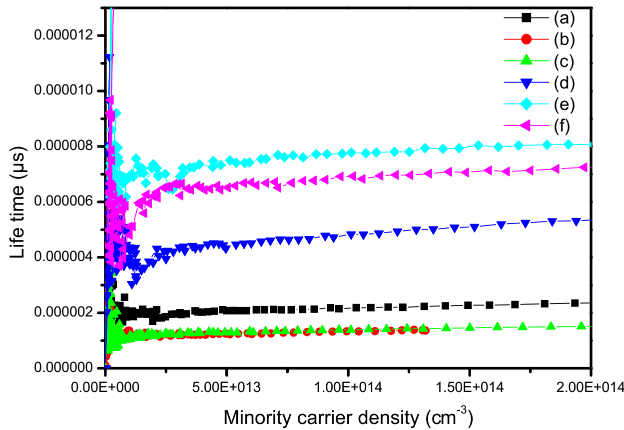

Fig. 7 Injection Dependent Lifetime Spectroscopy (IDLS) of (*a*) bare Si, (*b*) SiNWs, (*c*) pSiNWs and pSiNWs treated with different Li concentrations (*d*) C_1, (*e*) C_2 and (*f*) C_3

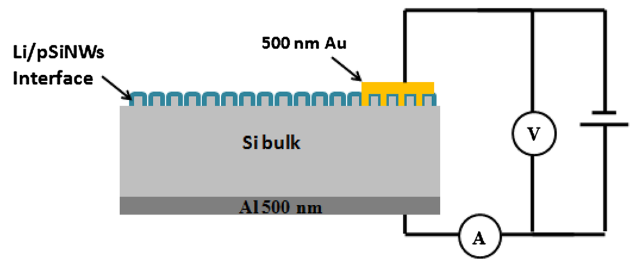

Fig. 8 Schematic illustration of the device used in the dark I–V measurements

effect of the pSiNWs by diminishing defect traps within the Si gap.

However when the Li concentration exceeds C_2, the minority carrier life time decreases slightly to 6.8 µs. This is mainly due to the generation of new lifetime killer centres by the formation of thick Li and oxide layers that cause the generation of dangling band at the interface $Si–SiO_2$. These new generated dangling bands act as the major recombination centres responsible for the observed lifetime degradation. This has been observed by Cui et al. [43] during the thermal treatment of Si and attributed to the generation of an excess of interstitial Si atoms during oxidation forming stacking faults at the $Si–SiO_x$ interface. Thus, we can conclude that the optimal Li concentration for passivation of pSiNWs is C_2 (Fig. 7).

4.7 The dark I–V characteristics

The effect of Li pore-filling with different concentrations (C_1, C_2, and C_3) on the electrical parameters of pSiNWs was analyzed using the dark current–voltage (I–V) characteristics. The metallic contacts are made by thermal evaporation under vacuum of Al for the rear contacts and Au for the emitter contacts. We used a thin Au layer on the front contact of the structure due to its high conductivity comparing to other usually used metals [44]. The metallic contacts are then annealed in an infrared furnace at 500 °C. The device used in the I–V measurements is described in Fig. 8. Measurements were performed a sandwich configuration, Au/Li–pSiNWs/Si/Al by applying voltage in respect Al as anode and Au as cathode. I–V characteristics were taken in air, in dry light, at room temperature.

Figure 9 presents dark I–V characteristics of Li-pSiNWs sandwich configuration. After Li pore-filling treatment, we note a significant improvement in the typical dark I–V characteristic with a good rectifying behavior. Additionally, we observe a decrease of the reverse current and significant increase in the forward current compared to the Li-free pSiNW sample which means that the rectifying behavior was improved after the Li treatment due to the hetero-junction potential barrier at the oxide /PSi interface. Figure 10 shows the rectifying ratio obtained at 5 V. The rectification ratio is defined as the ratio between forward current and the reverse current [45]. For the Li-free pSiNW sample, it is equal to 2.6, with increasing the Li concentration the rectification ratio gradually and reaches its maximum equal to 40.7 at C_2. The increase of the rectifying ratio after the Li pore-filling might be attributed to the formation of a thin oxide layer between the Au metal and the pSiNWs sidewalls. When exceeding this moderated concentration, the rectifying ratio decreases to 27 due to the formation of defect centers in the thick oxide layer. When the oxide

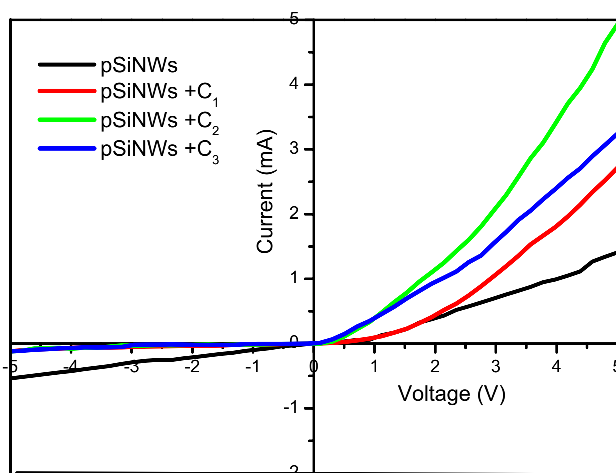

Fig. 9 Dark I–V characteristics of pSiNWs treated with Li at different concentrations

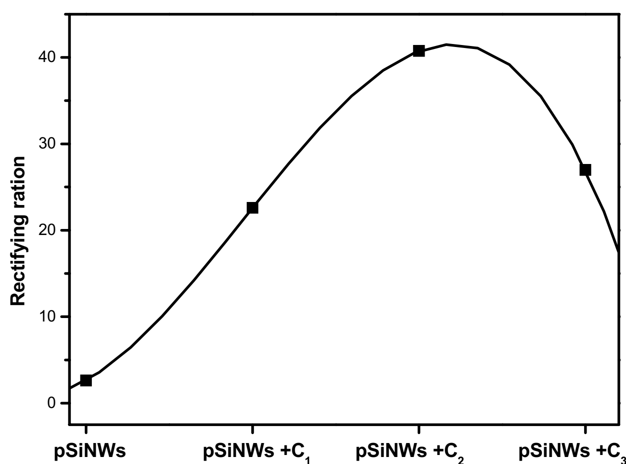

Fig. 10 Rectifying ratio versus Li concentration

Table 2 The variation of R_s as function of Li concentrations

Treatment condition	pSiNWs	pSiNWs + C_1	pSiNWs + C_2	pSiNWs + C_3
R_s (Ω)	340	156	85	273

layer becomes thicker enough, the tunneling probability of photo-carriers and the thermal generated carriers through the oxide layer are reduced leading to the reduction in the dark current.

To more qualify the improvement of the electrical parameters, we extract from the I–V characteristics the series resistances (R_s). For $(V-R_s \times I)>0$, the I–V characteristic can be approximated to a linear curve: $I \times \frac{dV}{dI} = I \times Rs$ [46]. Table 2 reveals the variation of R_s as function of Li concentrations. The R_s exhibits a significant decrease after Li pore-filling from 340 to 85 Ω for the concentration C_2. This is mainly attributed to the good passivation effect of the Li that reduces considerably the surface recombination. It is noted that both C_1 and C_3 Li concentration reduce R_s to 156 and 273 Ω, respectively. For the low LiBr concentration (C_1), the passivating layer leaves enough dangling bands. However, for high Li concentration (C_3) the passivating layer becomes relatively thick and causes the degradation of electrical proprieties. According to all these previous results, the Li immersion with moderated concentration leads to a good amelioration in the optoelectrical properties through the passivation of high dangling band density.

5 Conclusion

In this work, we use a simple, inexpensive and time saving method to produce luminescent pSiNWs with worthy electrical proprieties. The appearance of the PL emission from pSiNWs is attributed to the quantum confinement effect in the SiNCs generated within the porous structure. The post-chemical treatment of pSiNWs with Li pore-filling leads a fourfold PL intensity increase due to the passivation of high dangling band density and the amplification of the NBOHCs in the oxide layer. Additionally, the deposed Li film acts as light trapping layer leading to the dwindling of the total reflectivity from 4 to 1%. On the other hand, the effective minority carrier life time increases from 1.5 to 7.1 µs and the series resistance decreases from 340 to 85 Ω. In brief, the post chemical treatment combining AVE and Li pore-filling of SiNW enhances greatly their opto-electric performances and opens up opportunities for a new generation of pSiNW based opto-electronic and sensing devices.

Acknowledgements This study was supported by Laboratory of Semi-conductors, Nano-structures and Advanced Technologies (Grant No. 1).

References

1. M.T. Ahmadi, H. H. Lau, R. Ismail, V. K. Arora, Microelectron. J. **40**, 547 (2009)
2. G.-J. Zhang, Y. Ning, Anal. Chim. Acta **749**, 1 (2012)
3. B.-R. Hang, Y.-K. Yang, T.-C. Lin, W.-L. Yang, Sol. Energy Mater. Sol. Cells **98**, 357 (2012)
4. L. Lin, S. Guo, X. Sun, J. Feng, Y. Wang, Nanoscale Res. Lett. **5**, 1822–1828 (2010)
5. S. Li, W. Ma, Y. Zhou, X. Chen, Y. Xiao, M. Ma, W. Zhu, F. Wei, Nanoscale Res. Lett. **9**, 196–204 (2014)
6. C. Canevali, M. Alia, M. Fanciulli, M. Longo, R. Ruffo, C.M. Mari, Surf. Coat. Technol. **280**, 37–42 (2015)
7. L.T. Canham, Appl. Phys. Lett. **57**, 1046 (1990)
8. J.L. Gole, D.A. Dixon, Phys. Rev. B **57**, 12002 (1998)

9. M. Anutgan, T.A. Anutgan, I. Atilgan, B. Katircioglu, J. Lumin. **131**, 1305–1311 (2011)
10. C. Tsai, K.-H. Li, D.S. Kinosky, R.-Z. Qian, T.-C. Hsu, J.T. Irby, S.K. Banerjee, A.F. Tasch, J.C. Campbell, B.K. Hance, J.M. White, Appl. Phys. Lett. **60**, 1700 (1992)
11. L.T. Canham, T.I. Cox, A. Loni, A.J. Simons, Appl. Surf. Sci. **102**, 436–441 (1996)
12. M.V. Wolkin, J. Jorne, P.M. Fauchet, G. Allan, C. Delerue, Phys. Rev. Lett. **82**, 197 (1999)
13. A. Backes, U. Schmid, Sens. Actuators B **193**, 883–887 (2014)
14. H. Chen, R. Zou, H. Chen, N. Wang, Y. Sun, Q. Tian, J. Wu, Z. Chen, J. Hu, J. Mater. Chem. **21**, 801–805 (2011)
15. R.C. Wang, C.Y. Chao, W.S. Su, Acta Mater. **60**, 2097–2103 (2012)
16. S. Congli, H. Hao, F. Huanhuan, X. Jingjing, C. Yu, J. Yong, J. Zhifeng, S. Xiaosong, Appl. Surf. Sci. **282**, 259–263 (2013)
17. C. Amri, R. Ouertani, A. Hamdi, H. Ezzaouia, Superlattices Microst. **91**, 278–289 (2016)
18. L.H. Lin, S.P. Guo, X.Z. Sun, J.Y. Feng, Y. Wang, Nanoscale Res. Lett. **5**, 1822 (2011)
19. I. Leontis, A. Othonos, A.G. Nassiopoulou, Nanoscale Res. Lett. **8**, 383 (2013)
20. K. Li, X. Wang, P. Lu, J. Ding, N. Yuan, Nanoscale Res. Lett. **8**, 396 (2013)
21. S. Kato, Y. Kurokawa, S. Miyajima, Y. Watanabe, A. Yamada, Y. Ohta, Y. Niwa, M. Hirota, Nanoscale. Res. Lett. **8**, 361 (2013)
22. M. Saadoun, N. Mliki, H. Kaabi, K. Daoudi, B. Bessais, H. Ezzaouia, R. Bennaceur, Thin Solid Films **405**, 29–34 (2002)
23. L. Gan, L. Sun, H. He, Z. Ye, J. Mater. Chem. C **2**, 2668 (2014)
24. Y. Qu, L. Liao, Y. Li, H. Zhang, Y. Huang, X. Duan, Nano Lett. **12**, 4539–4543 (2009)
25. M.B. Rabha, W. Dimassi, M. Bouaïcha, H. Ezzaouia, B. Bessais, Sol. Energy **83**, 721 (2009)
26. A. Zarroug, I. Haddadi, L. Derbali, H. Ezzaouia, Superlattices Microstruct. **80**, 181–187 (2015)
27. I. Haddadi, S. Ben Amor, R. Bousbih, S. El Whibi, A. Bardaoui, W. Dimassi, H. Ezzaouia, J. Lumin. **173**, 257–262 (2016)
28. T. Saitoh, H. Hasegawa, Appl. Surf. Sci. **56**, 94–99 (1992)
29. R.E. Hollingsworth, J.R. Sites, J. Appl. Phys. **53**, 5357–5358 (1982)
30. S.M. Prokes, Appl. Phys. Lett. **62**, 3244 (1993)
31. F. Koch, Mat. Res. Soc. Symp. Proc. **298**, 319 (1993)
32. F. Koch, V. Petrova-Koch, T. Muschik, J. Lumin. **57**, 271 (1993)
33. S.M. Hossaina, S. Chakrabortya, S.K. Duttaa, J. Dasa, H. Saha, J. Lumin. **91**, 195–202 (2000)
34. A.S. Lenshin, P.V. Seredin, V.M. Kashkarov, D.A. Minakov, Mater. Sci. Semicond. Process. **64**, 71–76 (2017)
35. K. Peng, Y. Xu, Y. Wu, Y. Yan, S.-T. Lee, J. Zhu, Small **11**, 1062 (2005)
36. I. Haddadi, S.B. Slema, S.B. Amor, R. Bousbih, A. Bardaoui, W. Dimassi, H. Ezzaouia, J. Lumin. **160**, 176–180 (2015)
37. L.A. Dobrzański, M. Szindler, A. Drygała, M.M. Szindler, Cent. Eur. J. Phys. **12**(9), 666–670 (2014)
38. D. Li, S. Han, A. Li, Y. Wang, Y. Shan, F. Huang, Mater. Chem. Phys. **165**, 97–102 (2015)
39. M.H. Elshorbagy, K. Abdel-Hady, H. Kamal, J. Alda, Opt. Commun. **390**, 130–136 (2017)
40. J. Višniakov, A. Janulevičius, A. Maneikis, I. Matulaitienė, A. Selskis, M. Skapas, S. Stanionytė, A. Suchodolskis, Thin Solid Films **628**, 190–195 (2017)
41. A. Cuevas, D. Mcdonald, Sol. Energy **76**, 255–262 (2004)
42. J. Tang, J. Shi, L. Zhou, Z. Ma, Nano-Micro Lett. **3**, 129 (2011)
43. C. Cui, D. Yang, X. Yu, X. Ma, L. Li, D. Que, Microelectron. Eng. **66**, 373–378 (2003)
44. R.J. Martin-Palma, J.M. Martinez-Duart, L. Li, R.A. Levy, Mater. Sci. Eng. C **19**, 359–362 (2002)
45. K. Khan, S. Itapu, D.G. Georgiev, MRS Adv. **1**(49), 3341–3347 (2016)
46. D.K. Schroder, A Wiley-Interscience Publication, Arizona, Chap. 4, 147 (1990)